A wavenumber-partitioning scheme for two-dimensional statistical closures

J. C. Bowman

Institute for Fusion Studies, The University of Texas at Austin

Austin, Texas 78712

A technique of wavenumber partitioning that conserves both energy and enstrophy is developed for two-dimensional statistical closures. Coupled with a new time-stepping scheme based on a variable integrating factor, this advance facilitates the computation of energy spectra over seven wavenumber decades, a task that will clearly remain outside the realm of conventional numerical simulations for the foreseeable future. Within the context of the test-field model, the method is used to demonstrate Kraichnan's logarithmically-corrected scaling for the enstrophy inertial range and to make a quantitative assessment of the effect of replacing the physical Laplacian viscosity with an enhanced hyperviscosity.

I. INTRODUCTION

One of the principal advantages of statistical closure approximations for fluid turbulence is that they involve smoothly varying functions of wavenumber. This suggests the possibility of modeling a flow by following the evolution of only a few representative wavenumbers. This work presents two new techniques for the implementation of two-dimensional isotropic statistical closures that for the first time allows the inertial-range scalings of these approximations to be numerically demonstrated. The most interesting contribution is a rapidly converging mode reduction scheme that exploits the smoothness of the statistical variables in wavenumber space and conserves both energy and enstrophy. This scheme can be readily extended to handle anisotropic statistics (Bowman & Krommes 1995). The other advance reported here is a time stepping scheme based on a variable integrating factor that effectively removes one of two time scales from the integration of Markovian statistical closures. This new algorithm can reduce typical computation times for a Markovian closure by many orders of magnitude; however, since its discussion is of a more computational nature, we defer this topic to Appendix C.

The mode reduction scheme is based on the property that statistical quantities typically vary slowly in space compared with the primitive dynamical variables. Since the number of modes required for direct numerical simulation of high Reynolds number turbulence is enormous (Orszag 1970), the

DISCLAIMER

Portions of this document may be illegible in electronic image products. Images are produced from the best available original document.

possibility of dramatically reducing this number is one of the principal advantages afforded by statistical closures. The procedure introduces certain time-independent geometrical weight factors that are calculated as an initial computational overhead. These weight factors are used to evaluate new, effective mode-coupling coefficients that describe the interaction of certain statistically representative modes.

In Fourier space, the truncation wavenumber $k_{\max}$ should be chosen high enough so that in the wavenumber region $k > k_{\max}$ dissipation is dominant and turbulent activity is negligible. Truncation of the wavenumbers to a finite set destroys an infinity of invariants satisfied by the nonlinear terms. However, it is thought that only the lowest two invariants, the energy and enstrophy, play a significant role in determining the steady solutions of driven turbulence. At high Reynolds numbers, the cutoff wavenumber is usually taken to be much lower than what is actually justifiable, because of the lack of sufficient computer resolution to model the very small scales. To compensate in part for this truncation, an artificial dissipation mechanism known as a *hyperviscosity* is often introduced. Due to their superior scaling with $k_{\max}$, statistical closures can often be integrated over much wider inertial ranges than can their spectral-code counterparts. It is consequently not always necessary to adopt the artifice of hyperviscosity for closure computations. This allows an assessment of the true effect of a hyperviscosity on the large scale dynamics.

II. MODE REDUCTION

The mode reduction technique we are about to describe has its origins in a procedure originally used by Leith (1971) and Leith & Kraichnan (1972) to implement a phenomenological eddy-damped quasinormal Markovian [EDQNM] closure (Orszag 1977) and the test-field model [TFM] (Kraichnan 1971) for isotropic Navier-Stokes turbulence. Both techniques exploit the fact that statistical variables tend to vary slowly in wavenumber space compared with the rapid chaotic fluctuations of the (unaveraged) fundamental field. The variation of the statistical variables is determined largely by nonstochastic quantities like the linear forcing. While only a relatively small number of modes is required to model the linear forcing and the statistical quantities, many more will typically be required to model the mode-coupling effects properly. Since the latter effects are nonstochastic and time-independent, tremendous computational gains can be realized.

The wavenumber space is partitioned into bins (possibly nonuniformly spaced) over which the statistical variables are presumed to vary smoothly. Only a single representative mode is evolved from each bin. The number of interacting modes in each triad of wavenumber bins is accounted for by the introduction of enhanced coupling coefficients. These geometrical factors are independent of the fundamental dynamical variables and need only be computed once for each new wavenumber partition. The coarse-graining of wavenumber space "softens" the $\boldsymbol{k}+\boldsymbol{p}+\boldsymbol{q}=\boldsymbol{0}$ constraint: wavenumbers from

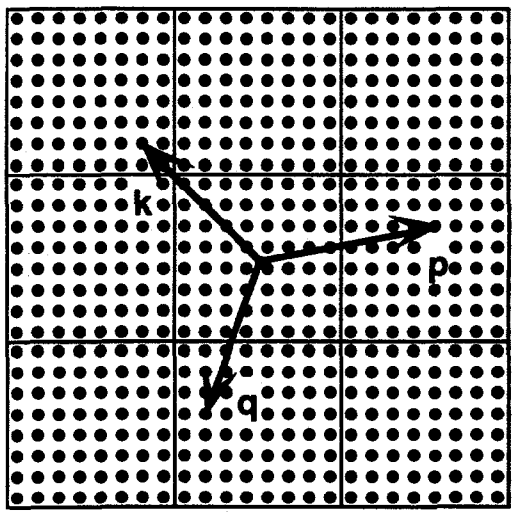

Figure 1: Coarse-graining of wavenumber space in a two-dimensional Cartesian bin geometry. The black dots represent individual modes.

two fixed bins will typically interact with wavenumbers located in several different bins (see Fig. 1). In contrast, the original $\boldsymbol{k}+\boldsymbol{p}+\boldsymbol{q}=\mathbf{0}$ constraint uniquely specifies a wavenumber $\boldsymbol{q}$ for each given combination of $\boldsymbol{k}$ and $\boldsymbol{p}$.

Quite generally, the advective nonlinearities encountered in turbulence will lead to rapidly varying mode-coupling coefficients. For example, the symmetrized mode-coupling coefficient will often contain rapidly varying factors such as q^2-p^2 and $\widehat{\boldsymbol{z}}\cdot\boldsymbol{p}\times\boldsymbol{q}$ that should be averaged along with the $\delta_{\boldsymbol{k}+\boldsymbol{p}+\boldsymbol{q},\mathbf{0}}$ convolution constraint. The computation of the bin-averaged mode-coupling coefficients is in general a nontrivial problem, particularly in non-Cartesian geometries.

For two-dimensional isotropic fluid turbulence written in Fourier space, it is natural to use polar coordinate geometry. Logarithmic spacing in the radial (wavenumber magnitude) direction is appropriate for modelling the power-law behaviour of an inertial range. Although the integration technique described in Appendix B will work for any grid spacing, there are also significant computational advantages in the use of a logarithmic grid, since one can then exploit various scaling properties of the weight factors.

The bin-averaging technique takes advantage of the relatively slow variation of the statistical variables with respect to wavenumber by passing to the limit of a continuum of modes. In this limit the computation of the bin-coupling coefficients becomes tractable. This can be accomplished either by taking the limit $L \to \infty$ of a discrete representation, in which $L^{-d} \sum_{\boldsymbol{k}} \to (2\pi)^{-d} \int d\boldsymbol{k}$, or equivalently by taking the Fourier integral transform of the original x-space system. Here d represents the dimension of the space and L represents a periodicity length in each Cartesian direction.

A. Bin-coupling coefficients

We now discuss the computation of the bin-coupling coefficients that characterize the interaction of the sample wavenumber modes.

To fix the notation, let us consider a quadratically nonlinear equation, written in Fourier space, for some stochastic variable $\psi_{\boldsymbol{k}}$ that has zero mean:

$$\left(\frac{\partial}{\partial t} + \nu_{\boldsymbol{k}}\right)\psi_{\boldsymbol{k}}(t) = \frac{1}{2}\frac{1}{(2\pi)^d}\int d\boldsymbol{p}\int d\boldsymbol{q}\, M_{\boldsymbol{kpq}}\psi^*_{\boldsymbol{p}}(t)\psi^*_{\boldsymbol{q}}(t). \qquad (1)$$

Here, the coefficients of linear "damping" $\nu_{\boldsymbol{k}}$ and mode-coupling $M_{\boldsymbol{kpq}}$ are time-independent. The $\delta(\boldsymbol{k}+\boldsymbol{p}+\boldsymbol{q})$ convolution constraint has been absorbed into $M_{\boldsymbol{kpq}}$. For simplicity, we will only discuss the case where the mode-coupling coefficients are real.

Without any loss of generality one may assume the symmetry

$$M_{\boldsymbol{kpq}} = M_{\boldsymbol{kqp}}. \tag{2}$$

Another important symmetry possessed by many such systems is

$$\sigma_{\boldsymbol{k}} M_{\boldsymbol{kpq}} + \sigma_{\boldsymbol{p}} M_{\boldsymbol{pqk}} + \sigma_{\boldsymbol{q}} M_{\boldsymbol{qkp}} = 0 \tag{3}$$

for some time-independent nonrandom real quantity $\sigma_{\boldsymbol{k}}$. Equation (3) is easily shown to imply that the nonlinear terms of (1) conserve the total generalized "energy," defined as

$$E \doteq \frac{1}{2} \int d\boldsymbol{k}\, \sigma_{\boldsymbol{k}} \left\langle |\psi_{\boldsymbol{k}}(t)|^2 \right\rangle . \tag{4}$$

(We emphasize definitions with the notation "$\doteq$".) The angle brackets in (4) denote an ensemble average. For some systems (*e.g.*, two-dimensional turbulence), (3) may be satisfied by more than one choice of $\sigma_{\boldsymbol{k}}$; this indicates the existence of more than one nonlinear invariant.

Typically, the mode-coupling coefficients satisfy the property that they vanish whenever any two of their indices are equal. Here we assume that this is the case, so that one may decompose

$$M_{\boldsymbol{kpq}} = A_{\boldsymbol{kpq}}\, \epsilon_{\boldsymbol{kpq}}, \tag{5}$$

where A_{kpq} is antisymmetric in $p \leftrightarrow q$, and ϵ_{kpq} is antisymmetric under permutation of any two indices. If we further restrict our attention to the case where M_{kpq} is a continuous function of its wavevector indices (on a specified domain), we may choose A_{kpq} (and ϵ_{kpq}) to be likewise continuous.

For example, if we adopt the normalization $\psi = k\bar{\psi}$, where $\bar{\psi}$ is the two-dimensional Navier-Stokes stream function, we identify

$$A_{kpq} = (q^2 - p^2), \tag{6a}$$

$$\epsilon_{kpq} = \left(\frac{\hat{z}\times p\cdot q}{kpq}\right)\delta(k+p+q). \tag{6b}$$

The symmetry of the factor ϵ_{kpq} is most readily seen by considering the triangle formed by the vectors k, p, and q; the factor $(\hat{z}\cdot p\times q)$ is just twice the area of the enclosed triangle. The formula $[s(s-k)(s-p)(s-q)]^{1/2}$ for the area of a triangle in terms of its semiperimeter $s \doteq (k+p+q)/2$ may be used to express this factor as a manifestly symmetric function of the three wavenumber magnitudes.

The form of A_{kpq} in (6a) is characteristic of any system that obeys two conservation laws. Without loss of generality, one may normalize ψ so that one of the invariants is obtained by setting $\sigma_k = 1$ in (4). Let the other invariant be associated with the quantity $\sigma_k = \xi_k$. From (3) and (5) we deduce the conservation relations

$$A_{kpq} + A_{pqk} + A_{qkp} = 0, \tag{7a}$$

$$\xi_k A_{kpq} + \xi_p A_{pqk} + \xi_q A_{qkp} = 0. \tag{7b}$$

A necessary and sufficient condition for (7) to have a solution is, upon noting the antisymmetry of A_{kpq},

$$(\xi_k - \xi_p)A_{kpq} = (\xi_q - \xi_p)A_{qpk}. \tag{8}$$

For $\xi_k = \xi_p$, (8) does not establish anything about the form of A_{kpq}. However, when $\xi_p = \xi_q$, (8) implies that $A_{kpq} = 0$. When $\xi_k \neq \xi_p$ and $\xi_p \neq \xi_q$, let us define

$$g_{kpq} \doteq \frac{A_{kpq}}{\xi_q - \xi_p}. \tag{9}$$

From the antisymmetry of A_{kpq} in $p \leftrightarrow q$ and (8), one deduces that g_{kpq} must be symmetric in all three indices. Without any loss of generality, one may therefore incorporate g_{kpq} into ϵ_{kpq}. This leaves us with the following general form for A_{kpq},

$$A_{kpq} = \xi_q - \xi_p. \tag{10}$$

Strictly speaking, this form is determined only when $\xi_k \neq \xi_p$; however, the assumed continuity of A_{kpq} implies that (10) is in fact valid for all choices of k, p, and q.

Let us define the equal-time correlation function $C_k(t) \doteq \left\langle |\psi_k(t)|^2 \right\rangle$, so that $E = \frac{1}{2}\int dk\, \sigma_k C_k(t)$. A typical second-order closure will prescribe evolution equations for C_k of the form

$$\frac{\partial C_k}{\partial t} + 2\nu_k C_k - 2 \sum_{k+p+q=0} M_{kpq} M_{pqk} \bar{\Theta}_{pqk} = \sum_{k+p+q=0} M_{kpq}^2 \bar{\Theta}_{kpq}, \tag{11}$$

where the statistical variable $\bar{\Theta}_{pqk}$ is some specified functional of C_k (and possibly other statistical variables as well).

If the continuum wavenumber space is divided into sufficiently small bins, the variation of the statistical quantities over each bin will be negligible. In a bin labeled by $\boldsymbol{K}$ with area $\Delta_{\boldsymbol{K}}$ one can then approximate the value of $C_{\boldsymbol{k}}$ by

$$C_{\boldsymbol{K}} \doteq \frac{1}{\Delta_{\boldsymbol{K}}} \int_{\Delta_{\boldsymbol{K}}} C_{\boldsymbol{k}}\, d\boldsymbol{k}. \tag{12}$$

(We will use upper-case indices like $\boldsymbol{K}$ to label the representative statistical mode associated with each bin.) Upon introducing the averaging operators (over bins $\boldsymbol{K}$, $\boldsymbol{P}$, and $\boldsymbol{Q}$)

$$\langle f \rangle_{\boldsymbol{KPQ}} \doteq \frac{1}{(2\pi)^d \Delta_{\boldsymbol{K}} \Delta_{\boldsymbol{P}} \Delta_{\boldsymbol{Q}}} \int_{\Delta_{\boldsymbol{K}}} d\boldsymbol{k} \int_{\Delta_{\boldsymbol{P}}} d\boldsymbol{p} \int_{\Delta_{\boldsymbol{Q}}} d\boldsymbol{q}\; \delta(\boldsymbol{k}+\boldsymbol{p}+\boldsymbol{q})\, f, \tag{13}$$

and (over bin $\boldsymbol{K}$)

$$\langle f \rangle_{\boldsymbol{K}} \doteq \frac{1}{\Delta_{\boldsymbol{K}}} \int_{\Delta_{\boldsymbol{K}}} d\boldsymbol{k}\, f, \tag{14}$$

we are led to consider a bin-averaged approximation of (11),

$$\begin{aligned} \frac{\partial C_{\boldsymbol{K}}}{\partial t} + 2\,\langle \nu_{\boldsymbol{k}} \rangle_{\boldsymbol{K}}\, C_{\boldsymbol{K}} \;-\; & 2 \sum_{P,Q} \Delta_{\boldsymbol{P}} \Delta_{\boldsymbol{Q}}\, \langle M_{\boldsymbol{kpq}} M_{\boldsymbol{pqk}} \rangle_{\boldsymbol{KPQ}}\, \bar{\Theta}_{\boldsymbol{PQK}} \\ = & \sum_{P,Q} \Delta_{\boldsymbol{P}} \Delta_{\boldsymbol{Q}} \left\langle M^2_{\boldsymbol{kpq}} \right\rangle_{\boldsymbol{KPQ}} \bar{\Theta}_{\boldsymbol{KPQ}}. \end{aligned} \tag{15}$$

In order to develop schemes that exactly conserve the energy and enstrophy, Leith (1971), Leith & Kraichnan (1972), and Bowman (1992) assumed that the asymmetric factor $A_{\boldsymbol{kpq}}$ of $M_{\boldsymbol{kpq}}$ varies slowly over a bin. However, for two-dimensional turbulence the asymmetric factor $(q^2 - p^2)$ actually changes sign as $\boldsymbol{p}$ and $\boldsymbol{q}$ are varied within the same bin! What results from

this crude approximation is a poorly convergent numerical scheme that mistreats nonlocal interactions (Pouquet *et al.* 1975). The principal contribution of the present work is the elimination of this assumption and the development of a more accurate reduction scheme.

There are two reasons why in their pioneering work, Leith and Kraichnan did not average the factor A_{kpq}. First, they apparently did not possess a general algorithm for computing $\langle f \rangle$, but only $\langle \epsilon_{kpq} \rangle$. Second, although the unaveraged equations (11) exactly conserve the energy and enstrophy, the bin-averaged equations (15) cannot simultaneously satisfy both laws, as we now illustrate.

Henceforth it will be convenient to incorporate the squared Jacobian factor ϵ_{kpq}^2, being symmetric in all three wavenumbers, into the averaging operation $\langle \cdot \rangle_{KPQ}$. While a linear average of (2) times A_{pqk} leads to the required energy conservation property

$$\langle A_{kpq} A_{pqk} \rangle_{KPQ} + \langle A_{pqk} A_{pqk} \rangle_{KPQ} + \langle A_{qkp} A_{pqk} \rangle_{KPQ} = 0, \qquad (16)$$

one cannot generally also satisfy the enstrophy conservation property

$$\xi_K \langle A_{kpq} A_{pqk} \rangle_{KPQ} + \xi_P \langle A_{pqk} A_{pqk} \rangle_{KPQ} + \xi_Q \langle A_{qkp} A_{pqk} \rangle_{KPQ} \neq 0, \quad (17)$$

for in general $\xi_K \langle f_{kpq} \rangle_{KPQ} \neq \langle \xi_k f_{kpq} \rangle_{KPQ}$. Thus, while the unaveraged equations conserve both energy and enstrophy exactly, (15) will violate one conservation law since the slowly varying approximation is not exact. Even a

weak violation of a conservation law will lead to improper cascades, nonlinear energy transfer, and inviscid (statistical-mechanical) equilibria.

In the previous work of Leith (1971), Leith & Kraichnan (1972), and Bowman (1992) only the symmetric factors $|\epsilon_{kpq}|$ or ϵ^2_{kpq} were averaged; consequently, these approximations do in fact conserve energy and enstrophy. However, there is an alternative and more accurate way of enforcing the energy and enstrophy symmetries. Let us define

$$\begin{aligned} S_{KPQ} &\doteq \langle A_{kpq} A_{pqk} \rangle_{KPQ} , \\ N_{KPQ} &\doteq \left\langle A^2_{kpq} \right\rangle_{KPQ} . \end{aligned} \tag{18}$$

What is required is a conservative approximation for

$$S_{KPQ} = \langle A_{kpq} A_{pqk} \rangle_{KPQ} \tag{19}$$

that is more accurate than the very crude estimate

$$S_{KPQ} = A_{kpq} A_{pqk} \langle 1 \rangle_{KPQ} \tag{20}$$

used in previous wavenumber partitioning schemes.

Energy and enstrophy conservation among the triad of bins K, P, Q require that

$$S_{KPQ} + N_{PQK} + S_{QPK} = 0 \tag{21}$$

and

$$\xi_K S_{KPQ} + \xi_P N_{PQK} + \xi_Q S_{QPK} = 0 \tag{22}$$

be satisfied simultaneously. This is possible if and only if

$$(\xi_K - \xi_P)S_{KPQ} = -(\xi_Q - \xi_P)S_{QPK}. \tag{23}$$

In other words, $(\xi_K - \xi_P)S_{KPQ}$ must be antisymmetric in $K \leftrightarrow Q$, in order for both conservation laws to hold exactly.

Two poor ways of achieving such an antisymmetry are the conventional approximation

$$(\xi_K - \xi_P)S_{KPQ} \approx (\xi_K - \xi_P)(\xi_Q - \xi_P)(\xi_K - \xi_Q)\,\langle 1\rangle_{KPQ} \tag{24}$$

and the crude antisymmetrization

$$\begin{aligned}(\xi_K - \xi_P)S_{KPQ} \;=\; \frac{1}{2}\Big[&(\xi_K - \xi_P)\,\langle(\xi_q - \xi_p)(\xi_k - \xi_q)\rangle_{KPQ} \\ &-(\xi_Q - \xi_P)\,\langle(\xi_k - \xi_p)(\xi_q - \xi_k)\rangle_{KPQ}\Big].\end{aligned} \tag{25}$$

The second approach so drastically alters the dynamics that it predicts incorrect inviscid statistical equilibria.

Fortunately, there is a more accurate way to antisymmetrize $(\xi_K - \xi_P)S_{KPQ}$ that does yield the correct statistical equilibria. Consider the approximation

$$(\xi_K - \xi_P)S_{KPQ} \approx \langle(\xi_k - \xi_p)(\xi_q - \xi_p)(\xi_k - \xi_q)\rangle_{KPQ} \tag{26}$$

obtained by inserting into the bin average the prefactor $(\xi_K - \xi_P) \equiv A_{QKP}$ instead of removing from it the two mode-coupling factors A_{kpq} and A_{pqk}. Equation (26) clearly satisfies the symmetry requirement (23).

But how good is this approximation? Clearly it is only reasonable when $\xi_K \neq \xi_P$. (The factor $\xi_k^2 - \xi_p^2$ changes sign as k and p are varied over the same bin.) Here we are extremely fortunate: the case $\xi_K = \xi_P$ is the very situation for which the conservation laws impose no restriction at all on the symmetries of S_{KPQ}; in this case $(\xi_K - \xi_P)S_{KPQ}$ vanishes and is anti-symmetric for any choice of S_{KPQ}! Thus, when $\xi_K = \xi_P$, one can evaluate $S_{KPQ} = \langle(\xi_q - \xi_p)(\xi_k - \xi_q)\rangle_{KPQ}$ exactly without violating any conservation laws. (26):

Consistency requirements then lead to the following approximation for S_{KPQ}:

$$S_{KPQ} = \begin{cases} \dfrac{\langle A_{kpq}A_{pqk}A_{qkp}\rangle_{KPQ}}{A_{qkp}} & \text{for } A_{QKP} \neq 0,\ A_{KPQ} \neq 0, \\ 0 & \text{for } A_{QKP} \neq 0, \quad A_{KPQ} = 0, \\ \langle A_{kpq}A_{pqk}\rangle_{KPQ} & \text{for } A_{QKP} = 0. \end{cases} \tag{27}$$

Having determined S_{KPQ}, one then computes N_{KPQ} from (21):

$$N_{KPQ} = -S_{QKP} - S_{PKQ} \tag{28}$$

This prescription leads to the expected inviscid equilibrium solutions for the bin quantities because it satisfies the required relation [*cf.* Bowman *et al.* (1993)]

$$\lambda_K N_{KPQ} + \lambda_P S_{KPQ} + \lambda_Q S_{KQP} = 0, \tag{29}$$

for $\lambda_K = \alpha + \beta\xi_K$, where α and β are any constants.

The implementation of this wavenumber partitioning scheme has resulted in a dramatic improvement in the convergence of the energy spectrum as the

resolution of the wavenumber partition is increased. The method is applicable to anisotropic statistics as well.

B. Geometric weight factors

The geometrical weight factors entering the summation in (15) account for the product of the areas of bins $\boldsymbol{P}$ and $\boldsymbol{Q}$ that interact to affect modes located within bin $\boldsymbol{K}$. To implement the bin-averaging procedure we therefore need to compute integrals of the following form over a polar grid:

$$\int_{k<}^{k>} k\,dk \int_{\alpha<}^{\alpha>} d\alpha \int_{p<}^{p>} p\,dp \int_{\beta<}^{\beta>} d\beta \int_{q<}^{q>} q\,dq \int_{\gamma<}^{\gamma>} d\gamma\, \delta(\boldsymbol{k}+\boldsymbol{p}+\boldsymbol{q})\, f(\boldsymbol{k},\boldsymbol{p},\boldsymbol{q}). \tag{30}$$

Here α, β, and γ are the respective angles of $\boldsymbol{k}$, $\boldsymbol{p}$, and $\boldsymbol{q}$ measured relative to some fixed reference. In making contact with the literature, note that these are related (but not identical) to the interior angles of the triangle formed by $\boldsymbol{k}$, $\boldsymbol{p}$, and $\boldsymbol{q}$. The relation between these two sets of angles is shown in Fig. 2. For isotropic turbulence, the angular limits of integration are $\alpha_< = \beta_< = \gamma_< = 0$ and $\alpha_> = \beta_> = \gamma_> = 2\pi$.

Kraichnan (1964), Leith (1971), and Leith & Kraichnan (1972) showed that the calculation can be greatly simplified by including only one factor of $(\hat{\boldsymbol{z}}\cdot\boldsymbol{p}\times\boldsymbol{q})^2$, namely $pq|\sin(\beta-\gamma)|$, in the bin average since this facilitates a natural change of variables from (p,β) to (p,q), where $q \doteq |\boldsymbol{k}+\boldsymbol{p}|$. That is, they chose $f(\boldsymbol{k},\boldsymbol{p},\boldsymbol{q}) = |\sin(\beta-\gamma)|/2k$. These authors approximately accounted for the contribution of the remaining factor by evaluating it at

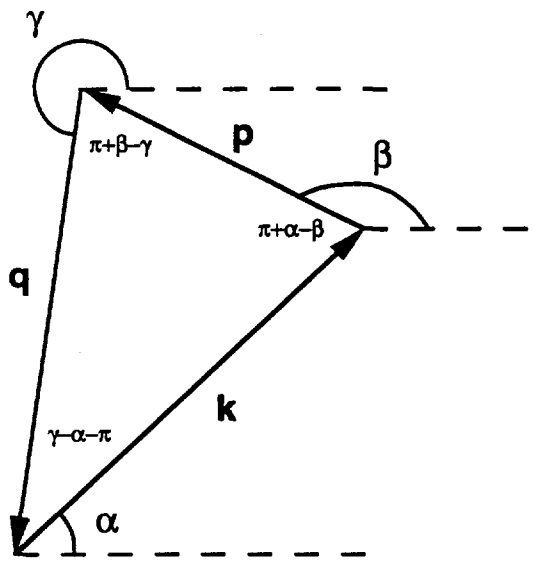

Figure 2: Relation between the angles associated with the convolution triangle.

the central wavenumbers $\boldsymbol{K}$, $\boldsymbol{P}$, and $\boldsymbol{Q}$. This introduces significant error since $|\sin(\beta-\gamma)|$ can vary rapidly over a bin. To partially compensate for this effect, they introduced subsidiary correction factors, which were approximately evaluated numerically. We will not discuss the details of these complexities since the general procedure to be described shortly will circumvent all of these difficulties.[1] However, this special case helps motivate our attack on the general problem (for an arbitrary f).

From an examination of the one-dimensional result found in Appendix A, one is led to consider the decomposition

$$\int_{k<}^{k>}\int_{p<}^{p>}\int_{q<}^{q>} = \left(\int_0^{k>} - \int_0^{k<}\right)\left(\int_0^{p>} - \int_0^{p<}\right)\left(\int_0^{q>} - \int_0^{q<}\right), \tag{31}$$

which reduces (30) to a sum of eight simpler integrals. The $\boldsymbol{q}$ integration can be performed trivially. For $f(\boldsymbol{k},\boldsymbol{p},\boldsymbol{q}) = |\sin(\beta-\gamma)|/2k$, each resulting integral has the form

$$\frac{1}{2}\int_0^{\Delta k} dk \int_0^{2\pi} d\alpha \int_0^{\Delta p} p\,dp \int_0^{2\pi} d\beta\ \mathrm{H}(\Delta q - |\boldsymbol{k}+\boldsymbol{p}|)\,|\sin(\beta-\gamma)|, \tag{32}$$

where now γ is the angle of $\boldsymbol{q} \doteq -(\boldsymbol{k}+\boldsymbol{p})$. Let us change variables from (p,β) to (p,q) so that $2q\,dq = -2kp\sin(\beta-\alpha)\,d\beta$, or, upon using the law of sines,

$$|p\,d\beta| = \left|\frac{dq}{\sin(\beta-\gamma)}\right|. \tag{33}$$

[1] In fact, we will eventually underscore the generality of our procedure by evaluating Leith's correction factors (*cf.* Table 2) exactly and comparing them to the true correction that results from averaging both Jacobian factors. In making this comparison, we will find significant differences. Leith and Kraichnan were aware of these discrepancies and attempted to correct for them by introducing yet another modification involving a phenomenological constant chosen to give the best fit for the inertial range.

We then find that

$$p\int_0^{2\pi} d\beta\,|\sin(\beta-\gamma)| = p\int_{\alpha-\pi}^{\alpha} d\beta\,|\sin(\beta-\gamma)| + p\int_{\alpha}^{\alpha+\pi} d\beta\,|\sin(\beta-\gamma)|$$
$$= 2\int_{|k-p|}^{k+p} dq. \tag{34}$$

Thus, (32) simplifies to

$$2\pi\int_0^{\Delta k} dk\int_0^{\Delta p} dp\int_{|k-p|}^{\min(k+p,\Delta q)} dq$$
$$= 2\pi\int_0^{\Delta k} dk\int_0^{\Delta p} dp\,[\min(k+p,\Delta q) - |k-p|], \tag{35}$$

which evaluates to the trilinear function (A14) of Δk, Δp, and Δq calculated in Appendix A.

We also include in Appendix A an interesting analytical solution to a one-dimensional case in which the corresponding weight function is $f(k,p,q)=1$. This formula could be used to compute the weight factor for a continuum two-dimensional Cartesian geometry by making use of the separability of the $\delta(\boldsymbol{k}+\boldsymbol{p}+\boldsymbol{q})$ function. In addition, the one-dimensional problem is equivalent to the isotropic two-dimensional problem (in polar geometry) for the case $f(\boldsymbol{k},\boldsymbol{p},\boldsymbol{q}) = 1/(4\pi^2 kp)$ since

$$\int_0^{2\pi} d\alpha\int_0^{2\pi} d\beta\int_0^{2\pi} d\gamma\, q\,\delta(\boldsymbol{k}+\boldsymbol{p}+\boldsymbol{q}) = \delta(k+p+q). \tag{36}$$

This technique could be applied to any isotropic function separable in the wavenumber magnitudes.

There appears to be no completely analytic solution to the general weight factor problem; instead, a combination of analytical and numerical techniques

is required. The calculation just outlined, particularly the reduction to (35), is an elegant algebraic alternative to the complicated geometric formulation of the problem given by Leith & Kraichnan (1972), who remark that the calculation "can be carried out as a straightforward but complex exercise in solid geometry and computer logic." The algebraic formulation has distinct advantages: first, it can be generalized to arbitrary integrands and, second, it is relatively easy to compute, as is described in Appendix B. Furthermore, it is straightforward to generalize this algorithm for modelling anisotropic turbulence on a polar grid; this is discussed by Bowman & Krommes (1995).

In Table 1 we demonstrate that our algorithm is in complete agreement with Table 1 of Leith & Kraichnan (1972); see Appendix A. In Table 2, we tabulate the exact values (accurate to the given number of digits) of the subsidiary correction factors that Leith and Kraichnan computed approximately and tabulated in their Table 2. Finally, we compare these correction factors to the true correction, tabulated in Table 3, that results from averaging both $(\widehat{\boldsymbol{z}}\cdot\boldsymbol{p}\times\boldsymbol{q})$ factors (as is done in the present work). The tabulated values are normalized in the same way as Leith's factors to facilitate comparison:

$$\bar{s}^{\text{actual}}_{\boldsymbol{KPQ}} \doteq \frac{\max(K,P,Q)}{2K^2P^2Q^2}\,\frac{\left\langle |pq\sin(\beta-\gamma)|^2\right\rangle_{\boldsymbol{KPQ}}}{\left\langle |\sin(\beta-\gamma)|/2k\right\rangle_{\boldsymbol{KPQ}}}. \tag{37}$$

For a log/linear partition, the central wavevectors $\boldsymbol{K}$, $\boldsymbol{P}$, and $\boldsymbol{Q}$ are constructed from the geometric means of the radial bin boundaries and the arithmetic means of the angular bin boundaries. We see that there are substantial differences between Leith's correction factors and the true correction.

j	i = 0	i = 1	i = 2	i = 3	i = 4
0	1.00000	1.00000	1.00000	1.00000	1.00000
1	1.00000	1.00000	1.00000	1.00000	1.00000
2	1.00000	1.00000	1.00000	1.00000	1.00000
3	1.00000	1.00000	1.00000	1.00000	0.92992
4	1.00000	1.00000	1.00000	0.92993	0.50000
5	1.00000	1.00000	0.98063	0.58651	0.09870
6	1.00000	1.00000	0.81399	0.21638	0.00047
7	1.00000	0.98693	0.52548	0.03106	0.00000
8	1.00000	0.90432	0.26284	0.00001	0.00000
9	1.00000	0.76577	0.10220	0.00000	0.00000
10	0.99946	0.60070	0.02521	0.00000	0.00000
11	0.97855	0.43976	0.00129	0.00000	0.00000
12	0.92205	0.31172	0.00000	0.00000	0.00000
13	0.84550	0.22042	0.00000	0.00000	0.00000
14	0.76057	0.15586	0.00000	0.00000	0.00000
15	0.67463	0.11021	0.00000	0.00000	0.00000

Table 1: Triangle volume fractions $\bar{v}(i,j)$ for the isotropic problem of Leith and Kraichnan.

All of these results were obtained merely by specifying different forms for the function f in the general algorithm described in Appendix B.

This algorithm is well suited to investigating the inertial-range scalings predicted by statistical closures for two-dimensional turbulence.

III. APPLICATION TO TWO-DIMENSIONAL TURBULENCE

The enstrophy inertial-range scaling for two-dimensional turbulence has been a subject of much controversy (*e.g.* McWilliams 1984; Santangelo *et al.* 1989; Benzi *et al.* 1990; Borue 1993; Bowman 1994). In this section we illus-

j	i = 0	i = 1	i = 2	i = 3	i = 4
0	0.90122	0.93055	0.95817	0.97605	0.98684
1	0.93055	0.95266	0.97966	0.99042	0.98662
2	0.95817	0.97966	0.99231	0.97190	0.91188
3	0.97605	0.99042	0.97190	0.88413	0.71825
4	0.98684	0.98662	0.91188	0.71826	0.54023
5	0.99208	0.96716	0.79870	0.57577	0.37584
6	0.99243	0.92707	0.68400	0.45424	0.15936
7	0.98787	0.86163	0.59663	0.32461	0.00000
8	0.97759	0.80176	0.52781	0.09375	0.00000
9	0.95960	0.75361	0.45663	0.00000	0.00000
10	0.92972	0.71766	0.35971	0.00000	0.00000
11	0.89513	0.69953	0.22445	0.00000	0.00000
12	0.87059	0.69337	0.00000	0.00000	0.00000
13	0.85292	0.68912	0.00000	0.00000	0.00000
14	0.83971	0.68561	0.00000	0.00000	0.00000
15	0.82952	0.68262	0.00000	0.00000	0.00000

Table 2: Exact values $\bar{s}^{\text{exact}}(i,j)$ of the subsidiary correction factors used by Leith and Kraichnan.

j	i = 0	i = 1	i = 2	i = 3	i = 4
0	0.88314	0.92489	0.95247	0.97037	0.98126
1	0.92489	0.97450	1.00253	1.01406	1.01089
2	0.95247	1.00253	1.01631	0.99663	0.93723
3	0.97037	1.01406	0.99663	0.90954	0.74714
4	0.98126	1.01089	0.93723	0.74712	0.57006
5	0.98666	0.99207	0.82633	0.60552	0.42501
6	0.98727	0.95284	0.71515	0.49469	0.20178
7	0.98312	0.88969	0.62893	0.37976	0.00000
8	0.97344	0.83371	0.56847	0.12056	0.00000
9	0.95639	0.78874	0.50548	0.00000	0.00000
10	0.92813	0.75482	0.41329	0.00000	0.00000
11	0.89641	0.74041	0.27676	0.00000	0.00000
12	0.87510	0.73981	0.00000	0.00000	0.00000
13	0.86052	0.74033	0.00000	0.00000	0.00000
14	0.85011	0.74069	0.00000	0.00000	0.00000
15	0.84238	0.74094	0.00000	0.00000	0.00000

Table 3: True corrections $\bar{s}^{\text{actual}}(i,j)$ obtained by properly averaging both $(\hat{\boldsymbol{z}}\cdot\boldsymbol{p}\times\boldsymbol{q})^2$ factors over each bin.

trate theoretical scalings by numerically solving the realizable test-field model [RTFM] (Bowman & Krommes 1995) and realizable Markovian closure [RMC] (Bowman *et al.* 1993) using the previously described techniques. For pedagogical reasons we will inject energy and enstrophy into the system only through a narrow wavenumber band. The numerical results were obtained with the generic code `DIA` (Krommes 1984; Krommes & Bowman 1988; Bowman 1992; Bowman & Krommes 1995), which uses a predictor-corrector algorithm to semi-implicitly advance the time step. The adjustable constant in the RTFM is arbitrarily taken to be 1.0; this value agrees well with the value 1.06 calculated for the TFM by Kraichnan (1971). His value was obtained by comparing the TFM to the direct-interaction approximation [DIA] (Kraichnan 1958, 1959, 1961) for interactions of comparable scales (when the DIA should be reliable).

A. Inviscid equilibria

Driven turbulence arises as a competition between dissipative linear forcing and the tendency of the nonlinearity to return the system to statistical equilibrium. Before considering the full problem of driven turbulence, it is advantageous to study the effects of dissipative linear forcing and nonlinear equilibration in isolation of each other. It is relatively trivial to verify the linear evolution. A more interesting study results from the removal of the linear growth and damping, so that one can focus solely on the interactions

of the nonlinear terms.

Following the equipartition arguments of statistical mechanics, Kraichnan (1967) proposed the discrete form

$$E_k = \frac{1}{2}\frac{1}{\alpha + \beta k^2} \tag{38}$$

for the steady-state spectrum of inviscid two-dimensional isotropic turbulence. This equilibrium form assumes that the dynamics is mixing, which is a plausible conjecture for systems with many interacting modes. In a continuum geometry, we need to include the volume element factor k:

$$E(k) = \frac{1}{2}\left(\frac{1}{2\pi}\right)\frac{k}{\alpha + \beta k^2}. \tag{39}$$

The inverse temperatures α and β can be determined from the initial conditions, as described in Appendix D. It is established in Appendix H of Bowman *et al.* (1993) that (38) is a steady-state solution to the statistical closures considered in this work. Figure 3 illustrates the relaxation predicted by the RMC closure to the equilibrium state (39), denoted by the solid curve. The temporal evolution of five representative modes is indicated with markers that grow larger as time proceeds. This represents an important and nontrivial test of the wavenumber partitioning scheme.

B. Driven two-dimensional fluid turbulence

Having considered the inviscid equilibrium problem, we now include the effects of linear forcing and viscous damping in the equation for the normal-

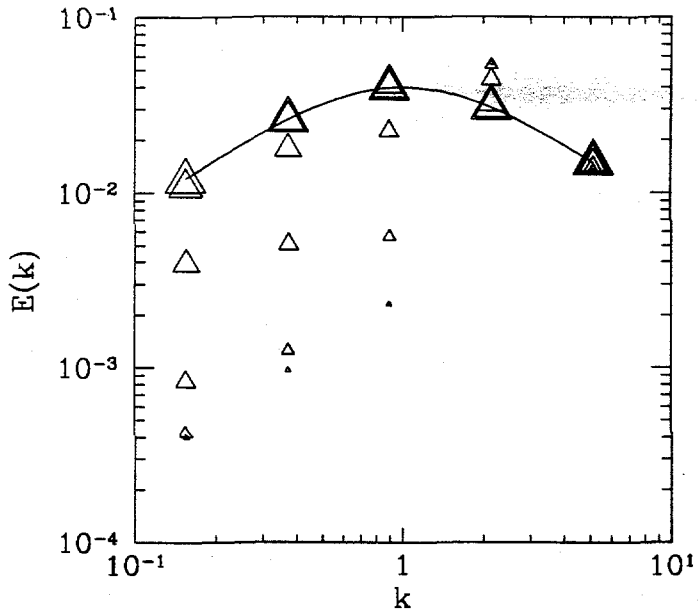

Figure 3: Relaxation of the inviscid Hasegawa-Mima problem to the equilibrium solution (39) for $\alpha = \beta = 1$.

ized variable ψ [*cf.* (6)]:

$$\frac{\partial}{\partial t}\psi_{\boldsymbol{k}} = \gamma_k \psi_{\boldsymbol{k}} + \frac{1}{2} \sum_{\boldsymbol{k}+\boldsymbol{p}+\boldsymbol{q}=0} (q^2 - p^2) \left(\frac{\widehat{\boldsymbol{z}} \cdot \boldsymbol{p} \times \boldsymbol{q}}{kpq} \right) \psi^*_{\boldsymbol{p}} \psi^*_{\boldsymbol{q}}. \tag{40}$$

The effects of short- and long-wavelength damping are modeled by the growth rate

$$\begin{aligned} \gamma_k &\doteq -\nu_L f_L(k) k^m - \nu_H f_H(k) k^n \\ &+ \begin{cases} \dfrac{\gamma_f}{\Delta_f} & \text{if } k_f - \frac{1}{2}\Delta_f < k < k_f + \frac{1}{2}\Delta_f, \\ 0 & \text{otherwise.} \end{cases} \end{aligned} \tag{41}$$

Choosing $m < 0$ and $n > 0$, the first two terms model damping at low and high wavenumbers, respectively. The functions $f_L(k)$ and $f_H(k)$, which would normally be set to unity, are introduced for use in the inertial-range studies described below. By restricting the injection of energy and enstrophy to a limited wavenumber band, we are readily able to follow the transfer of these quantities to other scales. The mechanism we use to inject energy into the system differs from the usual one in fluid turbulence studies. Energy is injected through a linear growth rate instead of an external random stirring force. The physical mechanism underlying the injection is not crucial to the concepts we wish to illustrate; we choose this method since it is appropriate for modeling the nonlinear fluid instabilities encountered in plasma physics.

Since the amount of enstrophy injection arising from the linear term of (40) depends on the fluctuation level, the calculation of the dissipation wavenumber k_d requires some knowledge of the steady-state energy spectrum. For an anticipated enstrophy inertial-range spectrum $E(k) = C_\zeta \zeta^\alpha k^\beta$,

the (wavenumber-independent) rate of enstrophy dissipation ζ is

$$\zeta = 2\nu_H \int_{k_f}^{\infty} k^{n+2} E(k)\, dk = 2\nu_H C_\zeta \zeta^\alpha \int_{k_f}^{k_d} k^{n+\beta+2}\, dk, \tag{42}$$

so that

$$\zeta^{1-\alpha} = 2\nu_H C_\zeta \left(\frac{k_d^{n+\beta+3} - k_f^{n+\beta+3}}{n+\beta+3} \right). \tag{43}$$

From the rate of enstrophy injection, $\zeta = 2\gamma_f k_f^2 E(k_f) = 2\gamma_f k_f^2 C_\zeta \zeta^\alpha k_f^\beta$, we deduce

$$\zeta^{1-a} = 2\gamma_f k_f^2 C_\zeta k_f^\beta. \tag{44}$$

Upon balancing the rates of enstrophy injection and dissipation, one then obtains a relation between ν_H and k_d,

$$\nu_H = \frac{(n+\beta+3)\gamma_f k_f^{\beta+2}}{k_d^{n+\beta+3} - k_f^{n+\beta+3}}. \tag{45}$$

Similarly, we determine a relation between ν_L and the energy dissipation wavenumber k_0 by balancing the rates of energy injection and dissipation over an anticipated energy inertial range of the form $E(k) = C_\epsilon \epsilon^{\alpha'} k^{\beta'}$,

$$\nu_L = \frac{(m+\beta'+1)\gamma_f k_f^{\beta'}}{k_f^{m+\beta'+1} - k_0^{m+\beta'+1}}. \tag{46}$$

The existence of true inertial ranges requires that the dissipation wavenumbers k_0 and k_d determined from (45) and (46) (in terms of the viscosity coefficients ν_L and ν_H) lie within the computational wavenumber domain.

For our first case study we introduce cutoffs to keep the dissipation ranges as narrow as possible by defining $f_L(k) = H(k_0 - k)$ and $f_H(k) = H(k - k_d)$,

where H is the Heaviside function. We choose the parameters

$$k_0 = 3.175, \quad k_d = 5.885 \times 10^5, \tag{47}$$

$$\nu_L = 0.25 \quad m = 0, \quad \nu_H = 1.0 \times 10^{-11}, \quad n = 2, \tag{48}$$

$$k_f = 4.416, \quad \Delta_f = 2.482, \quad \gamma_f = 1.733. \tag{49}$$

These parameters have been chosen to restrict the injection of energy and enstrophy to a single bin for a 24-bin configuration that spans the region between $k = 1$ and $k = 2^{20}$. The choice $n = 2$ corresponds to the true viscosity. The initial energy spectrum is chosen to be the statistical equilibrium spectrum given by (39) with $\alpha = \beta = 1$.

The saturated energy spectrum predicted by the RTFM is depicted by the solid line in Fig. 4, while the dotted line indicates the linear growth rate, which is plotted against the right-hand axis. The enstrophy inertial range is best demonstrated by examining the logarithmic slope of the energy spectrum (obtained by finite differencing), plotted as the solid line in Fig. 5.

Bowman (1994) has proposed a large-scale modification to Kraichnan's logarithmically corrected enstrophy inertial range law:

$$E(k) \sim k^{-3}\chi^{-1/3}(k) \qquad (k \geqslant k_1), \tag{50}$$

where $k_1 = k_f + \Delta_f/2$ and

$$\chi(k) \doteq \ln\left(\frac{k}{k_1}\right) + \chi_1. \tag{51}$$

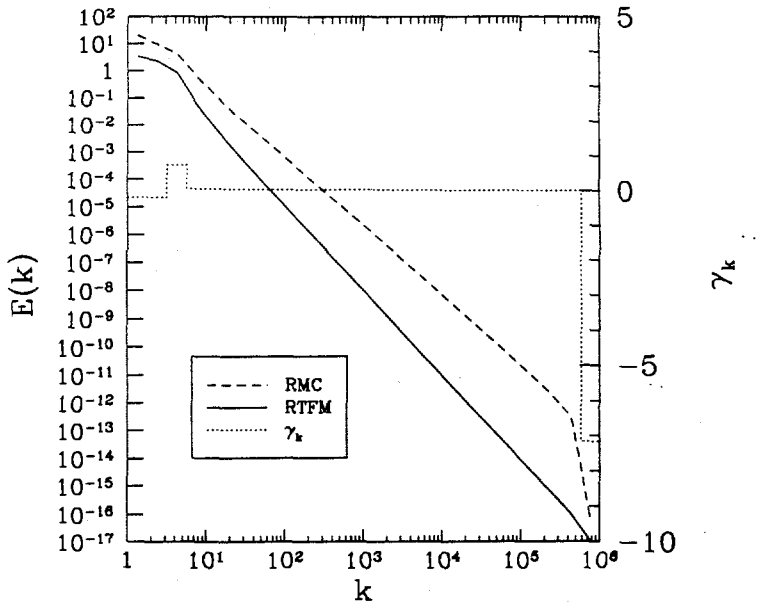

Figure 4: Saturated energy spectrum predicted by the RTFM and RMC.

The new constant χ_1, which removes the divergence from Kraichnan's law at the injection wavenumber, is set by the large-scale dynamics and cannot by determined by dimensional reasoning. To illustrate (50) we graph in Fig. 6 the "corrected slope," defined by

$$\frac{d \ln \left[E(k) \chi^{1/3} \right]}{d \ln k}, \tag{52}$$

for the value of the constant $\chi_1 = 0.46$ [determined by a least squares fit; for details, see Bowman (1994)]. In this manner, we obtain a constant corrected slope of -3.0 between $k = 50$ and $k = 10^5$.

The energy spectrum and slope predicted by the RMC for the same case is indicated by the dashed lines in Figs. 4 and 5. Instead of a logarithmically

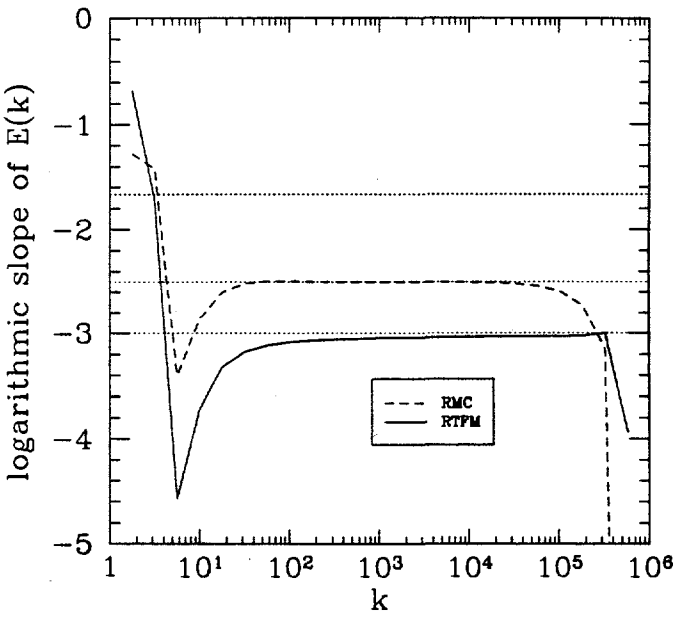

Figure 5: Logarithmic slope of the energy spectra predicted by the RTFM (solid line) and RMC (dashed line) in Fig. 4

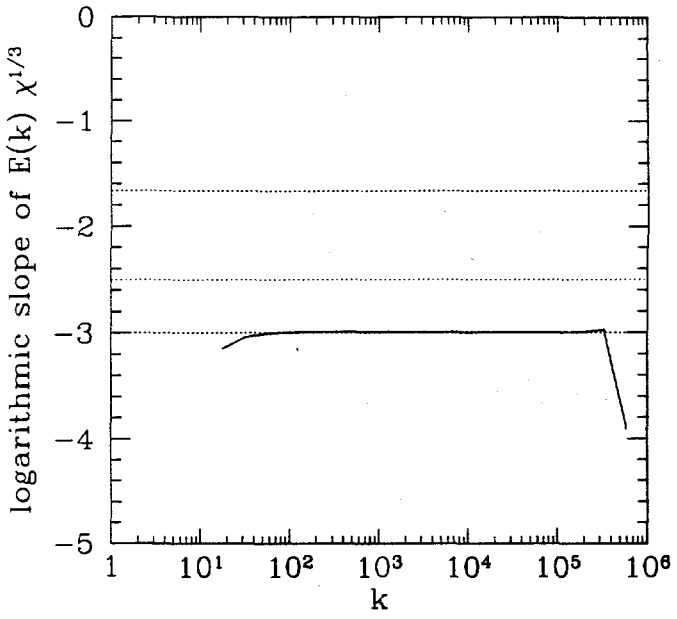

Figure 6: Corrected logarithmic slope of RTFM energy spectrum in Fig. 4.

corrected Kolmogorov exponent of -3, the value -2.5 is obtained. This is expected, since the RMC, like the DIA, is not invariant to random Galilean transformations of the fundamental variable.

It is instructive to compare these predictions with those obtained by a conventional bin-averaging scheme in which the factors A_{kpq} are evaluated outside the bin average. In Figs. 7 and 8 we observe the mistreatment of nonlocal interactions pointed out by Pouquet *et al.* (1975): for the RMC, an incorrect slope of -3 (with a logarithmic correction) is obtained. The RTFM appears to predict an insufficient amount of enstrophy dissipation for the formation of a proper inertial range. Moreover, even with modern

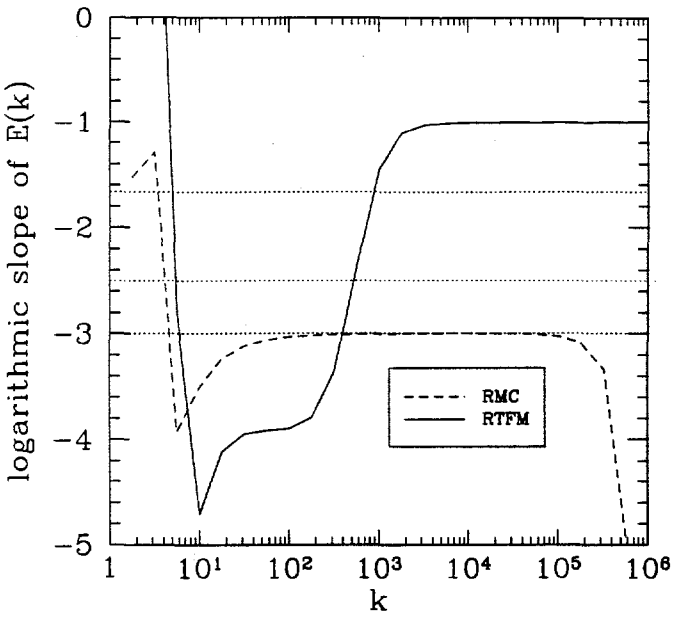

Figure 7: Logarithmic slope of the energy spectra for the RTFM and RMC using conventional bin-averaging.

computer resources, the total energy predicted by conventional methods does not appear to converge as the partition is refined.

In contrast, we see in Fig. 9 that even our highest resolution case, corresponding to a Reynolds number of about 10^{16}, converges even with a small number of bins; the energy spectra obtained with 32 bins and 64 bins very nearly coincide. To keep the dissipation range as narrow as possible, we introduce a hyperviscosity by setting $n = 6$ and $\nu_H = 3 \times 10^{-45}$. In Fig. 10 we compare the steady-state energy spectra obtained with this hyperviscosity and with the usual Laplacian viscosity given by $n = 2$ and $\nu_H = 2 \times 10^{-15}$. For these cases we remove the artificial dissipation cutoffs by setting $f_L = f_H = 1$.

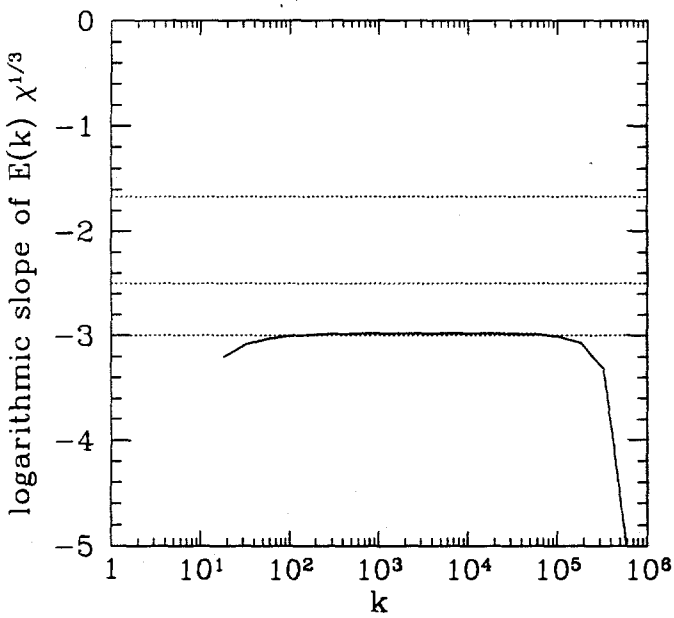

Figure 8: Corrected logarithmic slope of the energy spectrum for the RMC using conventional bin-averaging.

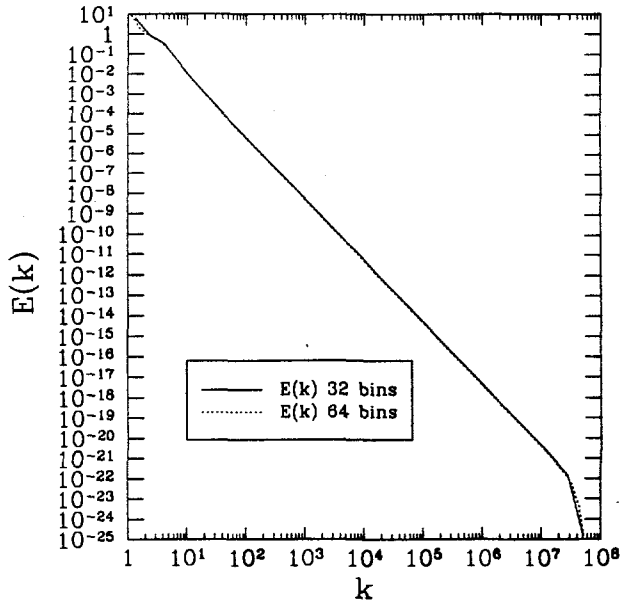

Figure 9: Convergence of wavenumber partitioning for high Reynolds number turbulence with hyperviscosity.

The usual justification for a hyperviscosity is based on the facts that the enstrophy transfer in the inertial range occurs only to the higher wavenumbers and the inverse energy transfer is negligible. Thus, it is argued, even a drastic modification to the dissipation dynamics cannot affect the slope of the inertial-range energy spectrum or the large scale dynamics. Upon examining Figs. 10 and 11 we see that this is indeed the case. For $n = 2$ ($n = 6$), the small-scale dissipation wavenumber k_d calculated from (45) is 2×10^7 (3×10^7), in good agreement with the wavenumbers at which the dissipation range is seen to begin in Fig. 11.

The efficiency of the numerical methods presented in this work is illus-

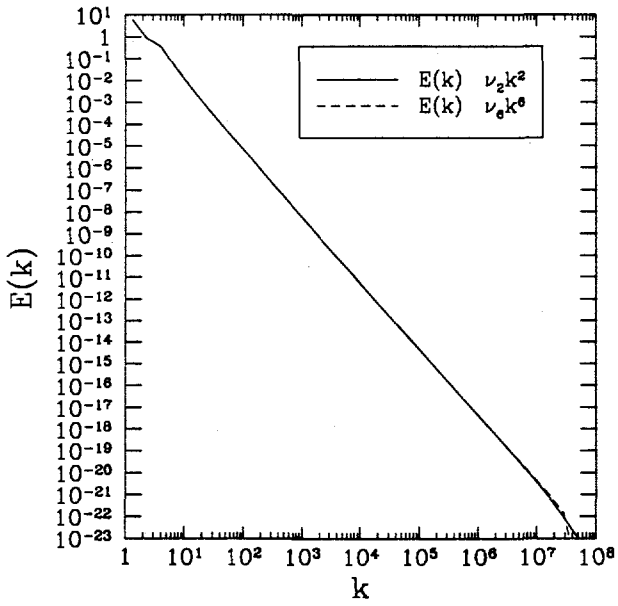

Figure 10: Comparison of energy spectra with Laplacian viscosity and hyperviscosity.

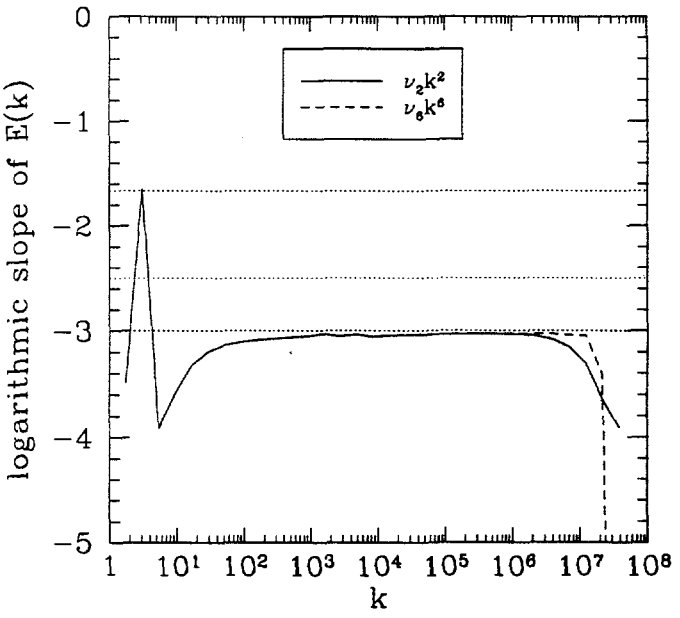

Figure 11: Logarithmic slopes of the energy spectra in Fig. 10.

trated by the fact that this high resolution hyperviscosity run required only 2.6 CPU hours on an RS6000 workstation. The number of distinct wavenumber triads associated with a 64 bin configuration is 10867. The computation of the corresponding bin-coupling coefficients used only 13 seconds of CPU time.

IV. DISCUSSION

One of the principal advantages of Markovian statistical closures is that the scaling of computation time with Reynolds number is superior to that for conventional numerical simulations. The ratio of the wavelengths of enstro-

phy injection and dissipation in two-dimensional turbulence is proportional to $R^{1/2}$. The uniform rate of enstrophy transfer in the inertial range implies that the ratio of the largest to smallest time scales must also be proportional to $R^{1/2}$. Thus, conventional simulations of two-dimensional turbulence require computation times proportional to $R^{3/2}$. In contrast, the number of logarithmically spaced bins required for a statistical closure computation scales as $\ln R^{1/2}$. If the bins are sufficiently small, the number of triads that must be evolved scales more like the square than the cube of the number of bins since the convolution constraint for the bin-averaging procedure reduces in this limit to the continuum form $\boldsymbol{k} + \boldsymbol{p} + \boldsymbol{q} = \boldsymbol{0}$. Thus the total computation time scales as $R^{1/2}(\ln R^{1/2})^2$, or simply as $R^{1/2} \ln^2 R$. Therefore, for sufficiently high Reynolds number turbulence, closure computations implemented with the wavenumber partitioning scheme will require much less effort than conventional simulations.

Because of their excellent scaling with Reynolds number, statistical closures are capable of modelling inertial ranges spanning many decades. They provides us with tools for investigating turbulence at extremely high Reynolds numbers (*e.g.* at the values of 10^{15} characteristic of atmospheric turbulence). For example, in this work we were able to demonstrate that the artifice of a hyperviscosity does not significantly alter the inertial-range dynamics and is therefore a valid technique for limiting the wavenumber domain, at least within the approximation of the realizable test-field model.

One would like to evaluate the role of coherent structures by comparing the accuracy of statistical closures for cases in which coherent structures are present to cases in which they are absent. Such a study might help settle the controversy surrounding the enstrophy inertial range in two-dimensional turbulence. If coherent structures played little role in determining the energy spectrum, this would be strengthen the case for Kolmogorov-type scalings.

The author acknowledges John A. Krommes and Maurizio Ottaviani for their participation in many stimulating discussions and their careful reading of early versions of this work. The author also thanks C. E. Leith for pointing out Pouquet's criticisms of the original partitioning scheme. Financial support was received from a Natural Sciences and Engineering Council of Canada Postdoctoral Fellowship and United States DoE contract No. DE–FG05–80ET–53088.

Appendix A. GEOMETRIC WEIGHT FACTORS: SPECIAL CASES

1. One-dimensional case

For the one-dimensional case where $f(k,p,q) = 1$, there is an interesting analytical solution to the weight factor problem. The form of the answer serves to motivate the solution of the general problem, (30).

Consider

$$\begin{aligned} I &\doteq \int_{k_<}^{k_>} dk \int_{p_<}^{p_>} dp \int_{q_<}^{q_>} dq\, \delta(k+p+q) \\ &= \int_0^{\Delta k} dk \int_0^{\Delta p} dp \int_0^{\Delta q} dq\, \delta(k+p+q+S), \end{aligned} \tag{A1}$$

with $\Delta k \doteq k_> - k_<$, $\Delta p \doteq p_> - p_<$, $\Delta q \doteq q_> - q_<$, and $S \doteq k_< + p_< + q_<$. Upon invoking the Inverse Fourier Theorem, we calculate

$$I = \int_0^{\Delta k} dk \int_0^{\Delta p} dp \int_0^{\Delta q} dq \int_{-\infty}^{\infty} \frac{d\alpha}{2\pi} e^{i\alpha(k+p+q+S)}$$

$$= \frac{-1}{2\pi i} \int_{-\infty}^{\infty} d\alpha \frac{e^{i\alpha S}}{\alpha^3} (e^{i\alpha\Delta k} - 1)(e^{i\alpha\Delta p} - 1)(e^{i\alpha\Delta q} - 1) \tag{A2}$$

$$= \frac{-1}{2\pi i} \int_{-\infty}^{\infty} d\alpha \frac{e^{i\alpha S}}{\alpha^3} \left[e^{i\alpha(\Delta k+\Delta p+\Delta q)} - e^{i\alpha(\Delta p+\Delta q)} - e^{i\alpha(\Delta k+\Delta q)} - e^{i\alpha(\Delta k+\Delta p)} + e^{i\alpha\Delta k} + e^{i\alpha\Delta p} + e^{i\alpha\Delta q} - 1 \right]. \tag{A3}$$

In the complex plane, consider the integral

$$\int_C d\alpha \frac{1}{\alpha^3} e^{i\alpha\lambda}, \tag{A4}$$

where C is a contour lying on the real axis deformed in a small semicircle above the pole at $\alpha = 0$. (This choice is arbitrary since it is clear from (A2)

that the final expression must be nonsingular.) We close this contour with a semicircle of radius R about the origin. For $\lambda > 0$, it is convenient to take the semicircle entirely in the upper-half plane since we may then make use of the well-known result that the contribution along the semicircular arc vanishes as $R \to \infty$. Since there are no poles within the enclosed contour, the integral along C must vanish. Similarly, for $\lambda < 0$ we choose the semicircular arc in the lower-half plane since now the contribution from this arc vanishes. In the latter case, we pick up a contribution to the integral along C from the residue at $\alpha = 0$:

$$\frac{1}{2}\frac{d^2}{d\alpha^2}e^{i\alpha\lambda}\Big|_{\alpha=0} = -\frac{1}{2}\lambda^2. \tag{A5}$$

Thus

$$\frac{1}{2\pi i}\int_C d\alpha\,\frac{1}{\alpha^3}e^{i\alpha\lambda} = \frac{1}{2}\lambda^2\mathrm{H}(-\lambda). \tag{A6}$$

The final result is then

$$\begin{aligned} I \\ = \; & -\frac{1}{2}[(k_> + p_> + q_>)^2\mathrm{H}(-k_> - p_> - q_>) - (k_< + p_> + q_>)^2\mathrm{H}(-k_< - p_> - q_>) \\ & -(k_> + p_< + q_>)^2\mathrm{H}(-k_> - p_< - q_>) - (k_> + p_> + q_<)^2\mathrm{H}(-k_> - p_> - q_<) \\ & +(k_> + p_< + q_<)^2\mathrm{H}(-k_> - p_< - q_<) + (k_< + p_> + q_<)^2\mathrm{H}(-k_< - p_> - q_<) \\ & +(k_< + p_< + q_>)^2\mathrm{H}(-k_< - p_< - q_>) - (k_< + p_< + q_<)^2\mathrm{H}(-k_< - p_< - q_<)]. \end{aligned} \tag{A7}$$

2. Leith's two-dimensional case

When $f(\boldsymbol{k},\boldsymbol{p},\boldsymbol{q}) = |\sin(\beta-\gamma)|/2k$, we noted in Sec. B that the weight factor

$$\begin{aligned} &J(k_<,k_>,p_<,p_>,q_<,q_>) \\ &\doteq \int_{k_<}^{k_>} k\,dk \int_0^{2\pi} d\alpha \int_{p_<}^{p_>} p\,dp \int_0^{2\pi} d\beta \int_{q_<}^{q_>} q\,dq \int_0^{2\pi} d\gamma\, \delta(\boldsymbol{k}+\boldsymbol{p}+\boldsymbol{q})\, f(\boldsymbol{k},\boldsymbol{p},\boldsymbol{q}), \end{aligned} \tag{A8}$$

reduces to the sum of eight integrals:

$$\begin{aligned} &J(k_<,k_>,p_<,p_>,q_<,q_>) \\ &= I(k_>,p_>,q_>) - I(k_>,p_>,q_<) - I(k_>,p_<,q_>) + I(k_>,p_<,q_<) \\ &\quad -I(k_<,p_>,q_>) + I(k_<,p_>,q_<) + I(k_<,p_<,q_>) - I(k_<,p_<,q_<), \end{aligned} \tag{A9}$$

where

$$I(\Delta k,\Delta p,\Delta q) \doteq 2\pi \int_0^{\Delta k} dk \int_0^{\Delta p} dp\,[\min(k+p,\Delta q) - |k-p|]. \tag{A10}$$

Let us now compute an explicit form for I.

Without loss of generality, order the wavenumbers so that $\Delta k \leqslant \Delta p \leqslant \Delta q$. By normalizing the wavenumber magnitudes to Δq, we may write $I = 2\pi\Delta q^3(I_1 - I_2)$, where

$$\begin{aligned} I_1 &\doteq \int_0^{k_0} dk \int_0^{p_0} dp \min(k+p,1), \\ I_2 &\doteq \int_0^{k_0} dk \int_0^{p_0} dp|k-p|, \end{aligned} \tag{A11}$$

with normalized limits $k_0 \doteq \Delta k/\Delta q$ and $p_0 \doteq \Delta p/\Delta q$.

The first integral evaluates to

$$\begin{aligned} I_1 &= \mathrm{H}(k_0+p_0-1)\left[-\frac{1}{6}k_0^3+\frac{1}{2}k_0^2-\frac{1}{2}k_0-\frac{1}{6}p_0^3+\frac{1}{2}p_0^2-\frac{1}{2}p_0+k_0p_0+\frac{1}{6}\right] \\ &\quad +\mathrm{H}(1-k_0-p_0)\left[\frac{1}{2}k_0p_0(k_0+p_0)\right]. \end{aligned} \tag{A12}$$

The second integral is

$$I_2 = \frac{1}{3}k_0^3-\frac{1}{2}k_0^2p_0+\frac{1}{2}p_0^2k_0. \tag{A13}$$

Upon combining these results, we obtain for the case $\Delta k \leqslant \Delta p \leqslant \Delta q$

$$\begin{aligned} \frac{1}{2\pi}I(\Delta k,\Delta p,\Delta q) &= -\frac{1}{6}\mathrm{H}(\Delta k+\Delta p-\Delta q)\Big[\Delta k(\Delta k^2-3\Delta k\Delta q+3\Delta q^2) \\ &\quad +\Delta p(\Delta p^2-3\Delta p\Delta q+3\Delta q^2)-\Delta q^3-6\Delta k\Delta p\Delta q\Big] \\ &\quad +\frac{1}{2}\mathrm{H}(\Delta q-\Delta k-\Delta p)\left[\Delta k\Delta p(\Delta k+\Delta p)\right] \\ &\quad +\frac{1}{2}\Delta k\Delta p(\Delta k-\Delta p)-\frac{1}{3}\Delta k^3. \end{aligned} \tag{A14}$$

By using this expression, we may then compute $J(k_<,k_>,p_<,p_>,q_<,q_>)$ using (A9).

We have verified that the results so obtained are in complete agreement with the data given in Table 1 of Leith & Kraichnan (1972) and with the identical Table 1 of this work, which was obtained with the general algorithm described in Appendix B. [Table 1 of Leith's earlier paper (Leith 1971) is incorrect.] The boundaries of the logarithmically spaced bins used by Leith and Kraichnan are given by

$$k_< = 2^{l/F}\delta^{-1}, \qquad k_> = 2^{l/F}\delta \tag{A15}$$

$$p_< = 2^{m/F}\delta^{-1}, \qquad p_> = 2^{m/F}\delta, \tag{A16}$$

$$q_< = 2^{n/F}\delta^{-1}, \qquad q_> = 2^{n/F}\delta, \tag{A17}$$

where $\delta \doteq 2^{1/2F}$ and l, m, and n are nonnegative integers. For the case $F = 4$, they tabulate the "triangle volume fraction"

$$\bar{\nu}(n-m, n-l) = \frac{1}{2\pi}\frac{J(k_<, k_>, p_<, p_>, q_<, q_>)}{(k_> - k_<)(p_> - p_<)(q_> - q_<)}. \tag{A18}$$

Note that the volume fraction depends on only two parameters due to the homogeneous scaling of $I(\Delta k, \Delta p, \Delta q)$.

For example, consider the case $l = 0$, $m = 6$, and $n = 8$, for which $\delta = 2^{1/8}$, $k_< = \delta^{-1}$, $p_< = 2\sqrt{2}\delta^{-1}$, and $q_< = 4\delta^{-1}$. Using (A9) and (A14) we calculate

$$\begin{aligned} J(k_<, k_>, p_<, p_>, q_<, q_>) &= -\sum_{h,i,j=0}^{1} (-1)^{h+i+j} I(\delta^{2h}k_<, \delta^{2i}p_<, \delta^{2j}q_<) \\ &= 0.097589, \end{aligned} \tag{A19}$$

which gives $\bar{\nu}(2, 8) = 0.26284$, in agreement with the value quoted by Leith & Kraichnan (1972) and tabulated in Table 1.

Appendix B. GEOMETRIC WEIGHT FACTORS: ISOTROPIC ALGORITHM

Here is the general algorithm used to compute the isotropic integral

$$\int_{k_<}^{k_>} k\,dk \int_0^{2\pi} d\alpha \int_{p_<}^{p_>} p\,dp \int_0^{2\pi} d\beta \int_{q_<}^{q_>} q\,dq \int_0^{2\pi} d\gamma\, \delta(\boldsymbol{k}+\boldsymbol{p}+\boldsymbol{q})\, f(\boldsymbol{k}, \boldsymbol{p}, \boldsymbol{q}), \tag{B1}$$

where α, β, and γ are the angles of $\boldsymbol{k}$, $\boldsymbol{p}$, and $\boldsymbol{q}$ respectively. The algorithm we are about to develop can actually be formulated for any function $f(\boldsymbol{k},\boldsymbol{p},\boldsymbol{q})$. However, in this discussion we will restrict f to be invariant to rigid rotations of all three wavevectors (*e.g.*, for the Navier-Stokes equation, f is in fact completely independent of the wavevector angles).

Evaluation of the innermost two integrals of (B1) yields

$$\int_{k_<}^{k_>} k\,dk \int_0^{2\pi} d\alpha \int_{p_<}^{p_>} p\,dp$$
$$\int_0^{2\pi} d\beta[\mathrm{H}(q_> - |\boldsymbol{k}+\boldsymbol{p}|) - \mathrm{H}(q_< - |\boldsymbol{k}+\boldsymbol{p}|)] f(\boldsymbol{k},\boldsymbol{p},-\boldsymbol{k}-\boldsymbol{p}). \quad \text{(B2)}$$

Upon introducing a change of angular variables from (α,β) to $(\alpha, r \doteq \beta - \alpha)$ and denoting $f(k,p,r) \doteq f(\boldsymbol{k},\boldsymbol{p},-\boldsymbol{k}-\boldsymbol{p})$, we may rewrite the integral as

$$\int_{p_<}^{p_>} p\,dp \int_{k_<}^{k_>} k\,dk$$
$$\int_{-2\pi}^{2\pi} dr\,[\mathrm{H}(q_> - |\boldsymbol{k}+\boldsymbol{p}|) - \mathrm{H}(q_< - |\boldsymbol{k}+\boldsymbol{p}|)]\,[\alpha_>(r) - \alpha_<(r)]\; f(k,p,r), \quad \text{(B3)}$$

where

$$\alpha_<(r) \doteq \begin{cases} 0 & \text{if } r \geqslant 0, \\ -r & \text{if } r < 0, \end{cases} \quad \text{(B4)}$$

$$\alpha_>(r) \doteq \begin{cases} 2\pi - r & \text{if } r \geqslant 0, \\ 2\pi & \text{if } r < 0. \end{cases} \quad \text{(B5)}$$

The problem has thus been reduced to a three-dimensional integration over p, k, and r. One can greatly speed up this calculation by eliminating unnecessary integration when the $\bar{r}$ integrand is zero due to the Heaviside restrictions

on $|\boldsymbol{k}+\boldsymbol{p}|$. This is accomplished by incorporating these restrictions explicitly into the limits of the r integration, as is discussed in detail for the general anisotropic algorithm by Bowman & Krommes (1995).

Efficient numerical integration requires some analytical knowledge of the behaviour of the integrand to determine the appropriate sampling resolution. An adaptive Simpson method is used to achieve a specified relative accuracy. To work correctly, the integration routine needs a resolution parameter $\Delta_{\max}$, which is set to the size of the smallest "structure" in the integrand (Bowman & Krommes 1995). Finally, we point out that any homogeneous scaling of the integrand with respect to k, p, and q should be exploited.

Appendix C. VARIABLE INTEGRATING FACTOR

The scalar equation

$$\frac{d\theta}{dt}+\eta\,\theta = S \tag{C1}$$

contains three time scales:

$$\eta^{-1} \quad \text{and} \quad \left(\frac{1}{\eta}\frac{d\eta}{dt}\right)^{-1} \text{and} \quad \left(\frac{1}{S}\frac{dS}{dt}\right)^{-1}. \tag{C2}$$

Given $\theta(t_0)$, we seek an approximation for $\theta(t_0+\Delta t)$ that avoids the restriction $\eta\,\Delta t \ll 1$ and hence computes the evolution on the time scale $n^{-1}(t_0)$ exactly.

Rewrite the matrix version of (C1) as

$$\frac{d\theta}{dt}+\eta(t_0)\,\theta = S+[\eta(t_0)-\eta(t)]\,\theta(t) \doteq Q(t). \tag{C3}$$

The exact solution for θ is

$$\theta(t) = P^{-1}(t) \int_0^t d\bar{t}\, \bar{P}\bar{Q}, \tag{C4}$$

where the integrating factor $P \doteq P(t)$ is defined by

$$\frac{dP}{dt} = P\,\eta(t_0), \qquad P(t_0) = 1. \tag{C5}$$

Hence

$$\theta(t_0 + \Delta t) = P^{-1}(t_0 + \Delta t) \left[\theta(t_0) + \int_{t_0}^{t_0+\Delta t} d\bar{t}\, \bar{P}\bar{Q}\right]. \tag{C6}$$

Since $d\bar{t}\, \bar{P} = d\bar{P}\, \bar{\eta}^{-1}$, a change of variables yields

$$\theta(t_0 + \Delta t) = P^{-1}(t_0 + \Delta t) \left[\theta(t_0) + \int_1^{P(t_0+\Delta t)} d\bar{P}\, \bar{\eta}^{-1}\bar{Q}\right]. \tag{C7}$$

The meaning of (C7) in the matrix case is elucidated upon writing it out in component form. Upon applying the trapezoidal approximation to $Q(P)$, one obtains

$$\theta(t_0 + \Delta t) = \\ P^{-1}(t_0 + \Delta t)\left[\theta(t_0) + \Big(P(t_0 + \Delta t) - 1\Big)\eta^{-1}(t_0)\left(\frac{Q(t_0) + Q(t_0 + \Delta t)}{2}\right)\right]. \tag{C8}$$

This leads to a time-stepping scheme that is correct to second order in Δt:

$$\begin{aligned}\theta(t_0 + \Delta t) \;=\; & P^{-1}(t_0 + \Delta t)\left[\theta(t_0) - \eta^{-1}(t_0)\left(\frac{Q(t_0) + Q(t_0 + \Delta t)}{2}\right)\right] \\ & + \eta^{-1}(t_0)\left(\frac{Q(t_0) + Q(t_0 + \Delta t)}{2}\right).\end{aligned} \tag{C9}$$

A standard predictor–corrector iteration is used to estimate $Q(t_0 + \Delta t)$.

The inverse integrating factor P^{-1} is computed exactly as

$$P^{-1}(t_0 + \Delta t) = \exp(-\eta(t_0)\,\Delta t). \tag{C10}$$

However, when the absolute values of the eigenvalues of $(\eta + \eta^\dagger)\Delta t$ are too small, some eigenvalues of P may be too close to unity for a numerically accurate implementation. In this case, the factor $(P-1)\eta^{-1}(t_0)$ in (C8) should be approximated by Δt; this reduces (C8) to the more familiar algorithm that results upon applying the trapezoidal approximation directly to (C6).

Algorithm (C6) can also be applied to the energy equation (15) by choosing $\eta = \langle \nu_k \rangle_K$ and incorporating the nonlinear damping into S. However, one cannot apply this method to the nonlinear damping term, even if it is proportional to C_K, since energy conservation requires that the nonlinear damping and source terms in (15) be treated on an equal footing.

If a dynamically-adjusted variable time step is used, (C9) can speed up realistic forced-dissipative turbulence computations by many orders of magnitude. It is particularly advantageous in the dissipation range, where the linear time scale is short compared to the nonlinear time.

Appendix D. CALCULATION OF INVERSE TEMPERATURES

Here we describe a procedure for determining the inverse temperatures α and β from the initial energy E_0 and enstrophy U_0,

$$E_0 = \frac{1}{2}\sum_{\boldsymbol{k}} \frac{1}{\alpha + \beta k^2}, \qquad U_0 = \frac{1}{2}\sum_{\boldsymbol{k}} \frac{k^2}{\alpha + \beta k^2}. \tag{D1}$$

We suppose that of $2N$ modes, only N are independent because of the reality condition $\psi_{-\boldsymbol{k}} = \psi_{\boldsymbol{k}}^*$.

The inversion can be done conveniently by expressing the ratio $r \doteq U_0/E_0$ in terms of $\rho \doteq \alpha/\beta$, using the relation $U_0 = (N - \alpha E_0)/\beta$. One finds

$$r = 2N\left[\sum_{\boldsymbol{k}} \frac{1}{\rho + k^2}\right]^{-1} - \rho. \tag{D2}$$

Upon inverting this equation for $\rho(r)$ with a numerical root solver, one may then determine α and β from the relations

$$\alpha = \frac{N}{E_0(r/\rho + 1)}, \qquad \beta = \alpha/\rho. \tag{D3}$$

REFERENCES

BENZI, R., PALADIN, G., & VULPIANI, A. 1990 Power spectra in two-dimensional turbulence. *Phys. Rev. A* **42**, 3654–3656.

BORUE, V. 1993 Spectral exponents of enstrophy cascade in stationary two-dimensional homogeneous turbulence. *Physical Review Letters* **71**, 3967–3970.

BOWMAN, J. C. & KROMMES, J. A. 1995 The realizable Markovian closure and realizable test-field model. II: Application to anisotropic drift-wave turbulence. to be submitted to *Phys. Fluids B.*

BOWMAN, J. C., KROMMES, J. A., & OTTAVIANI, M. 1993 The realizable Markovian closure. I: General theory, with application to three-wave dynamics. *Phys. Fluids B* **5**, 3558–3589.

BOWMAN, J. C. 1992 *Realizable Markovian Statistical Closures: General Theory and Application to Drift-Wave Turbulence.* Ph.D. thesis Princeton University Princeton, NJ.

BOWMAN, J. C. 1994 On inertial-range scaling laws. submitted to *J. Fluid Mech.*

KRAICHNAN, R. H. 1958 Irreversible statistical mechanics of incompressible hydromagnetic turbulence. *Phys. Rev.* **109**, 1407–1422.

KRAICHNAN, R. H. 1959 The structure of isotropic turbulence at very high Reynolds numbers. *J. Fluid Mech.* **5**, 497–543.

KRAICHNAN, R. H. 1961 Dynamics of nonlinear stochastic systems. *J. Math. Phys.* **2**, 124–148.

KRAICHNAN, R. H. 1964 Decay of isotropic turbulence in the direct-interaction approximation. *Phys. Fluids* **7**, 1030–1047.

KRAICHNAN, R. H. 1967 Inertial ranges in two-dimensional turbulence. *Phys. Fluids* **10**, 1417–1423.

KRAICHNAN, R. H. 1971 An almost-Markovian Galilean-invariant turbulence model. *J. Fluid Mech.* **47**, 513–524.

KROMMES, J. A. & BOWMAN, J. C. 1988 `DIA`: A code to solve the anisotropic direct-interaction approximation. *Bull. Am. Phys. Soc.* **33**, 2022.

KROMMES, J. A. 1984 "Topics in the theory of statistical closure approximations for plasma physics" in *Statistical Physics and Chaos in Fusion Plasmas*, edited by Horton, C. W. & Reichl, L. E. pp. 241–252 Wiley, New York.

LEITH, C. E. & KRAICHNAN, R. H. 1972 Predictability of turbulent flows. *J. Atmos. Sci.* **29**, 1041–1058.

LEITH, C. E. 1971 Atmospheric predictability and two-dimensional turbulence. *J. Atmos. Sci.* **28**, 145–161.

MCWILLIAMS, J. C. 1984 The emergence of isolated coherent vortices in turbulent flow. *J. Fluid Mech.* **146**, 21–43.

ORSZAG, S. A. 1970 Analytical theories of turbulence. *J. Fluid Mech.* **41**, 363–386.

ORSZAG, S. A. 1977 "Lectures on the statistical theory of turbulence" in *Fluid Dynamics*, edited by Balian, R. & Peube, J.-L. pp. 236–373 Gordon and Breach, London (summer school lectures given at Grenoble University, 1973).

POUQUET, A., LESIEUR, M., ANDRÉ, J. C., & BASDEVANT, C. 1975 Evolution of high Reynolds number two-dimensional turbulence. *J. Fluid Mech.* **72**, 305–319.

SANTANGELO, P., BENZI, R., & LEGRAS, B. 1989 The generation of vortices in high-resolution, two-dimensional decaying turbulence and the influence of initial conditions on the breaking of self-similarity. *Phys. Fluids A* **1**, 1027–1034.